Article

Upward Fire Spread Hazard of Vertical Greenery Systems: A Comparative Study with External Thermal Insulation Composite System and Double-Skin Façade

Tharindu Lakruwan Wickremanayake Karunaratne [ID] **and Cheuk Lun Chow *** [ID]

Department of Architecture and Civil Engineering, City University of Hong Kong, Hong Kong, China; tkarunara2-c@my.cityu.edu.hk
* Correspondence: cheuchow@cityu.edu.hk; Tel.: +852-3442-9858

Abstract: Recent studies have shown that vertical greenery systems (VGS) carry a significant fire threat when not properly looked after. Building on this, the fire hazard of VGS was compared to two other thermally efficient building façade systems (TEBFS), namely external thermal insulation composite systems (ETICS) and double-skin façade (DSF). Numerical simulations were conducted in the fire dynamic simulator (FDS). A fire initiated as a room fire of 1 MW followed by a window-ejected flame on a 12 m tall and 9 m wide front façade with a TEBFS. Three scenarios for each TEBFS were simulated for better comparison. Rapid upward fire spread (UFS) was observed in the VGS scenarios, recording average UFS rates of 8.97, 5.51 and 2.86 cms^{-1} compared to the scenarios of the other 2 TEBFS where the flame failed to reach the top of the façade within the stipulated simulation time of 300 s. The maximum temperatures reached along the façade in VGS scenarios were much higher than those in the other two TEBFS. In conclusion, the fire hazard of VGS in certain conditions is much higher compared to the fire scenarios of ETICS and DSF that are scrutinised by building codes in many countries for fire safety.

Keywords: upward fire spread; external thermal insulation composite system (ETICS); double-skin façade (DSF); vertical greenery system (VGS); fire dynamic simulator (FDS)

1. Introduction

In hot and humid climates, heat transfer through building façades is found to have the most considerable effect on building energy performance [1]. In addition, building façade systems with better thermal performance provide better thermal comfort for the occupants due to a more stable indoor thermal environment [2]. Unfortunately, there is a well-established concern regarding the fire hazard attached to TEBFS [3]. An external thermal insulation composite system (ETICS) façade [4,5] and a double-skin façade (DSF) [6,7] are two of the TEBFS of which the fire hazard has been extensively studied over the years. When the compartment fire of a building reaches the fully developed stage, there is a risk of flames ejecting out of broken glass windows. This phenomenon facilitates fire spread in high-rise buildings from floor to floor [8]. Having a façade system that facilitates the spread of flames or hot gases to the upper floors could potentially escalate the damage caused by the fire in other compartments of the building.

The design of a DSF could lead to fire problems, and failure to comply with fire safety codes is seen with many DSF projects [9,10]. The fire hazard related to a DSF is high because hot gases trapped inside the vertical air cavity can move upwards rapidly in a channel flow. Experimental results have indicated that the cavity width in a DSF is a vital factor influencing plume trajectory [6,11]. The driving force, which determines the attachment of the plume to the interior or the exterior skin, is created by the difference in pressure between the two sides of the window plume [12]. Whether the flame is impinging on the inner or outer glass pane is an important phenomenon to study as it defines the level of

fire hazard associated with the DSF. The breakage of glass on either skin is undesirable. However, flames impinging on the inner glass panes on the upper floors is riskier as the smoke and flame moving out to the cavity might spread to the adjacent levels [6]. Full-scale experimental and simulation results with DSF models with cavity widths of 0.5, 1.0 and 1.5 m have revealed that which glass pane breaks first, the outer or inner, depends on the cavity width [13,14].

Organic insulation materials such as extruded polystyrene (XPS), expanded polystyrene (EPS) and polyurethane (PUR) foam used in ETICS ignite and melt when exposed to heat and contribute to the rapid spread of fire [15]. Ensuring fire safety is difficult in buildings with excessive insulation, as the materials undergo rapid combustion with high heat-release rates (HRR) while releasing massive volumes of smoke carrying toxic gases [16]. Incidents that occurred in Television Central Culture (TVCC) in Beijing, Wanxin Complex in Shenyang and Grenfell Tower in London are some examples of fires that were aggravated by insulation material [17,18]. Full-scale studies focused on the UFS of ETICS are rare in the literature, mainly due to the high cost of conducting large-scale façade fire tests [19]. However, the fire hazard of individual components (organic thermal insulation materials, in particular) of these composites has been studied in the past [20–23].

VGS are currently gaining popularity as a building façade application to minimise the impact of the urban heat island effect (UHE) along with noise and sound pollution inside the buildings of urban settings [24]. VGS are also capable of providing passive energy benefits in the form of shadow through the vegetation layer, insulation through the vegetation layer and the substrate, and evaporative cooling through evapotranspiration [25]. The general understanding is that VGS are not a fire threat as long as they are properly looked after to keep them green and alive [26]. Hence, studies focused on the fire hazard of VGS are scarce in the published literature. However, there have been a few recent studies that show how much of a threat VGS would pose if they are not adequately maintained [27–29]. The MC and the packing ratio (PR) are the two most important factors that govern the flammability characteristics of a vegetation-full bed of a single species [30]. The level of fire hazard when the foliage of VGS is not kept fresh and lush is highlighted in these studies.

In this study, the upward fire spread (UFS) is defined as the flow of flames or hot gases from a lower level of a building to an upper level after window flame ejection. Once the flame is ejected from a window, the subsequent UFS depends on the façade system that is present in the building. Fire spread could take either the form of UFS along the surface of materials or the upward spread of hot gases in a channel through the structure of a TEBFS. When there is a TEBFS with flammable materials, the former scenario occurs, while a TEBFS, like a DSF, could facilitate the latter. The fire hazard of TEBFS is shown in Figure 1.
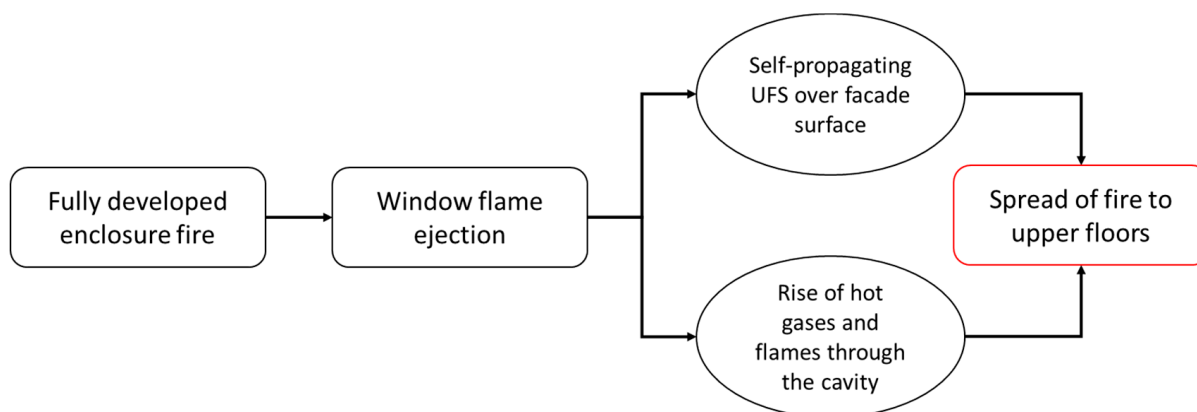

Figure 1. The fire hazard of TEBFS.

With this backdrop, this study aims to further investigate the fire hazard of VGS by comparing them with two of the more established façade fire phenomena of the ETICS façade and DSF. A numerical simulation methodology was followed for this study due to the high cost and time attached to conducting repetitive real-scale façade fire tests. Numerical simulations were conducted in the fire dynamic simulator (FDS) version 6.7.5 developed by NIST [31]. FDS is widely accepted in the fire safety engineering community for fire modelling with a significant amount of validation work [32]. Three scenarios for each TEBFS were simulated by changing the expanded polystyrene (EPS) layer thickness in ETCIS, cavity width in DSF and moisture content (MC) of vegetation in VGS for better comparison of the results. Three scenarios from each TEBFS were selected to represent a high, medium and low level of fire hazard.

2. Numerical Simulation of Upward Fire Spread of Thermally Efficient Building Façade Systems

2.1. Overview of the FDS Model

A four-storey building with a TEBFS on one side of the façade was simulated. The dimensions of the building were set as 9 m × 6 m × 12 m (width × depth × height) with a storey height of 3 m. A broken window was modelled on the first floor as an opening of 1 m × 1 m, from where a fire plume emerged due to a flashover fire scenario in the compartment. The window was placed in a way so that the centreline of the window and the centreline of the TEBFS coincided in the vertical axis. The base of the window was at a height of 3 m from the bottom (Figure 2).
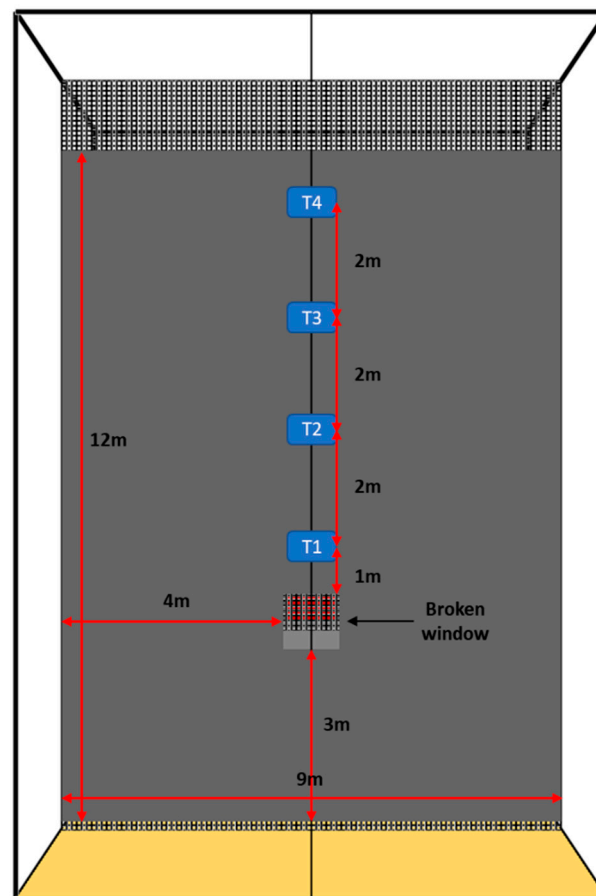

Figure 2. Location of temperature devices along the TEBFS.

A fire was modelled to occur at the far corner (from the TEBFS) of the first floor, from a surface of 1 m × 1 m facing the direction of the TEBFS. The perpendicular distance from this fire surface to the inner surface of the façade was 5.8 m in all the simulation scenarios.

From this surface, a fire size of 1 MW, which is similar to that involving a "moderate-weight type B upholstered furniture" item (Table 3.6 in Karlsson and Quintiere [33]) in an enclosure fire, was achieved in the simulation by setting the HRR per unit area (HRRPUA in kWm^{-2}) in FDS to 1000. The temperature distribution along the vertical centreline of the TEBFS was recorded by placing temperature devices above the window at four heights: 5 m (T1), 7 m (T2), 9 m (T3) and 11 m (T4) from the base of the building (Figure 2). These are "wall temperature" devices in FDS that measure the solid phase surface temperature. The devices were placed on the outer surface of the façade in ETICS and on the outer surface of the inner pane in DSF. In VGS scenarios, particles were introduced at the above heights and in line with the outer boundary of the VGS façade to hold the devices, as a solid surface is not available.

FDS calculations are performed on a domain made out of rectilinear volumes known as meshes. These meshes are divided into rectangular cells with a sufficient resolution to capture the flow dynamics. In FDS, $D^*/\delta x$ gives a measure of how well the flow field is resolved [31]. Here, D^* is the characteristic fire diameter and δx is the nominal size of a mesh cell. D^* is defined as:

$$D^* = \left(\frac{\dot{Q}}{\varrho_\infty c_p T_\infty \sqrt{g}} \right)^{\frac{2}{5}}. \tag{1}$$

where $\dot{Q}$ is the heat release rate of the fire, ϱ_∞ is the ambient air density (kg m^{-3}), c_p is the specific heat (kJ kg^{-1} K^{-1}) and T_∞ ambient temperature (K). For an optimum mesh resolution, the $D^*/\delta x$ ratio should be between 4 and 16, giving results at a satisfactory level of accuracy and within reasonable computational time [34]. When the $D^*/\delta x$ ratio is less than 4, the results may have unfavourable accuracy, while a ratio greater than 16 may result in longer computational times. For the current study the $D^*/\delta x$ ratio for a cell size of 10 cm was 9.59, which is acceptable.

In addition to the above calculation, a mesh sensitivity study was conducted using three computational grids for one scenario each from the three TEBFS. An ETICS with an EPS layer thickness of 5 cm, a DSF with a cavity width of 1 m and a VGS with an MC of 30% were selected for this purpose.

The mesh sensitivity study was started with a coarser mesh with a cell size of 20 cm (M1) and then followed by relatively finer meshes with cell sizes of 10 cm (M2) and 5 cm (M3). The total number of cells in M1, M2 and M3 was 2.25×10^5, 1.8×10^6 and 1.44×10^7, respectively.

The temperature recordings of the device T1 were compared among the 3 selected simulation scenarios, which showed a significant deviation in the results of the 2 meshes, M1 and M2, as seen in Figure 3. The results between the 2 meshes, M2 and M3, showed very little deviation (Figure 3). However, the simulation time for mesh M3 was significantly higher compared to the simulation time for mesh M2 for all 3 simulation scenarios. This outcome is also in line with the mesh resolution calculation, where the $D^*/\delta x$ ratios of the 3 meshes were 4.79, 9.59 and 19.18 respectively. Hence, mesh M2 was selected as the optimum mesh with a cell size of 10 cm to obtain accurate results within a feasible simulation time.

2.2. Details of the Scenarios Simulated

The three TEBFS simulated in this study are the ETICS façade, the DSF and the VGS wall. Figure 4 shows the geometrical models of the building with the 3 façade types in FDS. The same building structure was used for all three scenarios while only changing the front façade of the building to demonstrate the three different TEBFS. As the simulated building façade was external and facing ambient conditions, open vents were used on the exterior mesh boundaries.
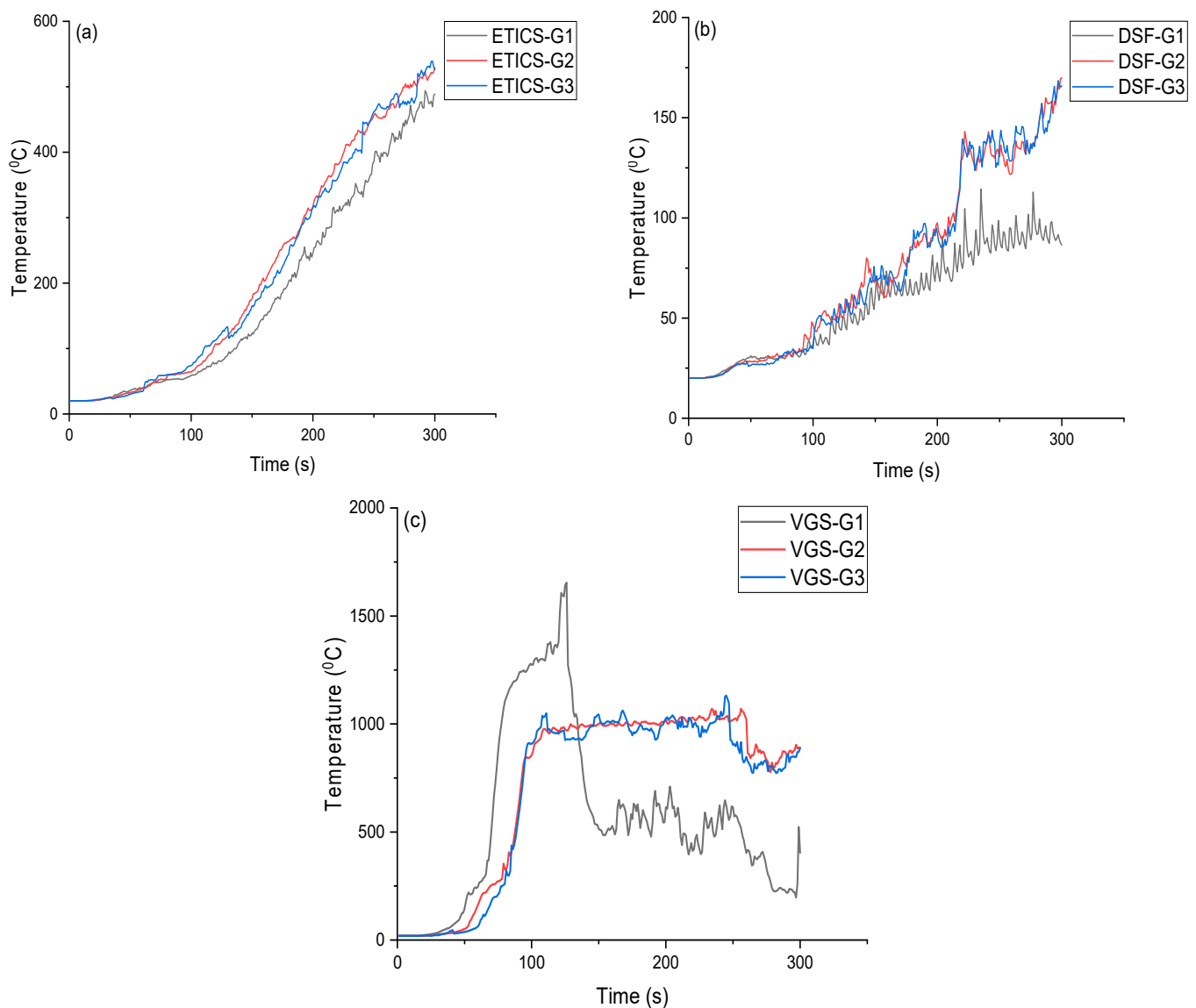
Figure 3. Grid sensitivity analysis of (**a**) ETICS, (**b**) DSF, (**c**) VGS.

The ETICS façade was considered to consist of three layers from exterior to interior as polymer cement mortar (PCM), cement mortar (CM) and EPS core, respectively [35]. The 3 layers are not visible in Figure 4a, as all 3 layers were included under the same "SURF" namelist in the FDS input file as different layers of material. The "SURF" namelist in FDS is used to prescribe the boundary conditions for the solid obstructions [31]. The cavity of the DSF in Figure 4b is covered on the sides by galvanised steel plates and was opened from the top and the bottom. This DSF model was adopted from a DSF test rig used in 2 previous studies [14,36], reflecting the actual DSF setup. The VGS wall in Figure 4c was modelled as a collection of vegetation particles packed within a thickness of 10 cm [29].

Three scenarios each from the three TEBFS were simulated for better comparison of the results. The EPS thickness in the ETICS façade, cavity width in DSF, and MC in VGS were varied to obtain different scenarios under each TEBFS. The details of the differentiating parameter of the 3 scenarios under each TEBFS, and the sources from which these scenarios are selected, are given in Table 1.

Table 1. Differentiating parameters for different simulation scenarios.

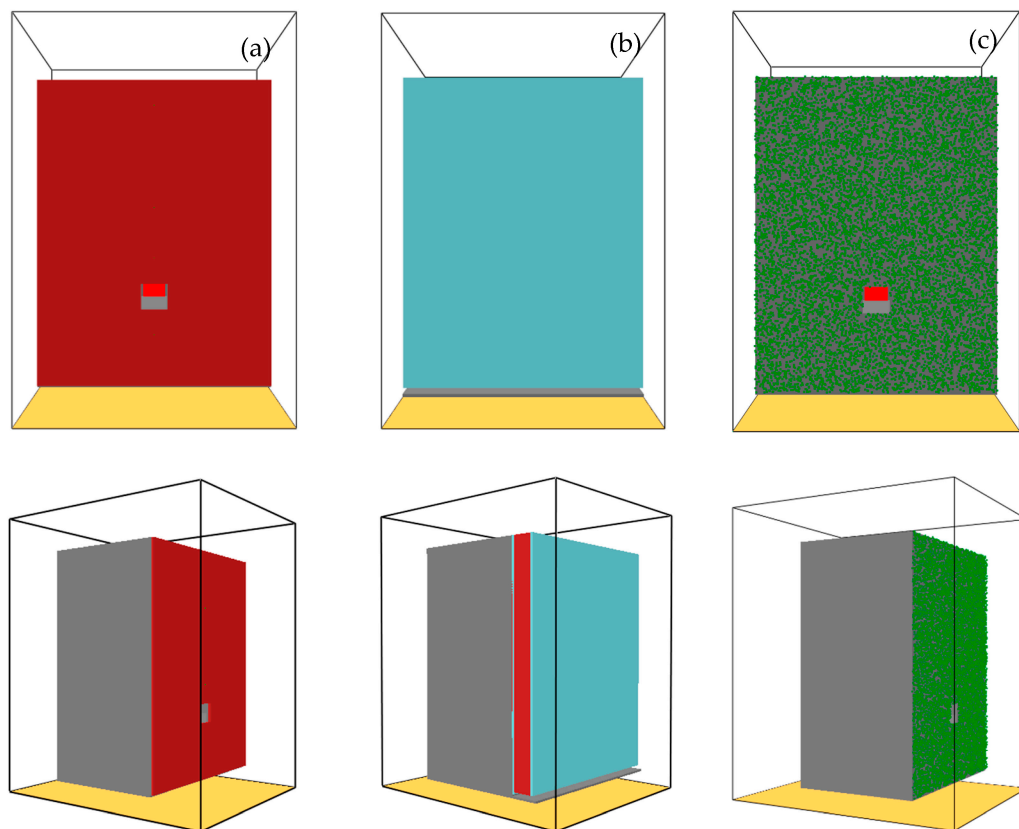| TEBFS	Differentiating Parameter			Sources
ETICS façade	EPS thickness			
	ETICS1	ETICS2	ETICS3	
	5 cm	10 cm	20 cm	[35]
DSF	Cavity Width			
	DSF1	DSF2	DSF3	
	0.5 m	1 m	1.5 m	[6,13,14,36]
VGS	Vegetation MC			
	VGS1	VGS2	VGS3	
	30%	50%	80%	[27]

Figure 4. FDS building model of (**a**) ETICS façade, (**b**) DSF, (**c**) VGS wall.

The other physical parameters of the 3 TEBFS used in the FDS simulations are given in Table 2. The values of these parameters remained constant in each of the three simulation scenarios under the respective TEBFS.

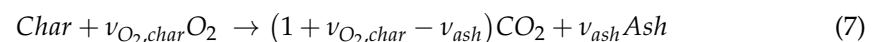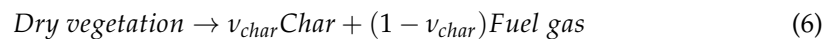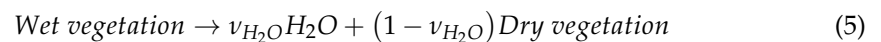The reaction model of the ETICS façade was demonstrated using 3 chemical reactions [35].

$$PCM \rightarrow SBR + CM \tag{2}$$

$$EPS \rightarrow PS_m \tag{3}$$

$$PS_m \rightarrow PS_g \tag{4}$$

Table 2. Physical parameters of the simulation scenarios.

Parameter	Value
ETICS	
PCM thickness	0.002 m
CM thickness	0.001 m
DSF	
Glass dimensions (L × W × T)	11.5 m × 9 m × 0.10 m
Bottom vent height	0.15 m
VGS	
PR	0.50
Particle dimensions (L × W × T)	0.04 m × 0.04 m × 0.01 m
VGS wall thickness	0.10 m
Number of vegetation particles in the VGS wall	1,070,000 particles
Particle density of the VGS wall	100,000 particles/m^3
Bulk density of vegetation in the VGS wall	50 kg m^{-3}

In reaction (2), *PCM* is pyrolyzed to produce 5.97% of styrene–butadiene rubbers-latex (*SBR*) gaseous fuel and 94.03% of solid *CM*. Thereafter, the *EPS* layer receives heat through the *CM* layer and undergoes two chemical reactions. *EPS* melts in the reaction (3) and the resulting molten polystyrene (PS_m) is decomposed to produce gaseous polystyrene (PS_g).

On the other hand, the pyrolysis process of vegetation in the VGS wall in FDS is characterised by 3 pyrolysis reactions [31]:

$$Wet\ vegetation \rightarrow v_{H_2O}H_2O + (1 - v_{H_2O})Dry\ vegetation \tag{5}$$

$$Dry\ vegetation \rightarrow v_{char}Char + (1 - v_{char})Fuel\ gas \tag{6}$$

$$Char + v_{O_2,char}O_2 \rightarrow (1 + v_{O_2,char} - v_{ash})CO_2 + v_{ash}Ash \tag{7}$$

Here, v_{H2O} is the mass fraction of water within the solid or the moisture fraction (MF), v_{char} is the mass fraction of dry vegetation that is converted to char during pyrolysis, v_{ash} is the mass fraction of char that is converted to ash during char oxidation and v_{O2}, char is the mass of oxygen required per unit mass of char consumed. Reaction (5) expresses the process of fresh vegetation drying to produce dry vegetation and water vapour. In reaction (6), the remaining dry vegetation undergoes further decomposition by emitting gaseous fuel (volatile pyrolyzates) and residual char. Finally, reaction (7) shows the oxidation of the residual char by emitting CO_2 and leaving out only ash.

2.3. Input Parameters of the FDS Model

The thermal and physical properties of the materials and the kinetic constants of all the chemical reactions are necessary as input parameters for the FDS simulations. The values for the 3 scenarios simulated are given in Table 3.

For the conductivity of PS_m and for the specific heat of *EPS*, PS_m, dry vegetation, char and ash, the relevant expressions capture the variation of the temperature in the FDS simulations.

It is essential to specify the kinetic constants of all the chemical reactions incorporated in the FDS input file to define the rate of reaction at a particular temperature. The important kinetic constants are the pre-exponential factor (A) and the activation energy (E). The kinetic constants for the 6 reactions in the 3 scenarios are given in Table 4.

Table 3. Material properties.

Material	Density (kg m^{-3})	Conductivity (Wm^{-1} k^{-1})	Specific Heat
		ETICS	
PCM	1000 [35]	0.4 [35]	1.420 [35]
CM	1200 [35]	$2 - 2.45 \times 10^{-3}T + 1.07 \times 10^{-6}T^2$ [35]	0.880 [35]
EPS	15 [35]	0.038 [35]	$1470 + 5T$ [35]
PS$_m$	1200 [35]	$0.2 + 6 \times 10^{-5}T$ [35]	$1710 + 0.7T$ [37]
		VGS	
Dry vegetation	100 [27]	0.21 [38]	$0.1031 + 0.003867T$ [39]
Char	300 [31]	0.05 [31]	$0.42 + 0.002T + 6.85 \times 10^{-7}T^2$ [40]
Ash	67 [31]	0.1 [31]	$1.244 \left(\frac{T}{300} \right)^{0.315}$ [41]
		DSF	
Glass	2000	0.8	0.840
Galvanised steel	7800	52	0.470

Table 4. Values of the kinetic constants of the reactions.

Reaction	A	E (J/mol)
PCM pyrolysis (R1)	1.68×10^6 [35]	9.42×10^7 [35]
EPS melting (R2)	1.6×10^{-2} [35]	0 [35]
PS melt decomposition (R3)	1.16×10^8 [35]	1.73×10^8 [35]
Moisture evaporation (R4)	600,000 [31]	48,200 [31]
Vegetation pyrolysis (R5)	36,300 [31]	60,300 [31]
Char oxidation (R6)	430 [31]	74,800 [31]

3. Results and Discussion

3.1. Upward Fire Spread along the TEBFS

The time-varied temperature readings of the 4 temperature read-out devices during the simulation time (300 s) were analysed to understand the UFS in all the simulated scenarios. The temperature–time curves of all the devices for every simulation scenario of ETICS and DSF are plotted separately. These results are helpful in identifying the ETICS and DSF scenarios with the most significant UFS hazard.

Figure 5 shows the temperature recorded by the 4 devices (T1–T4) for the 3 scenarios of ETICS1, ETICS2 and ETICS3 with EPS thicknesses of 5 cm, 10 cm and 20 cm, respectively.

The variation in temperature recorded by the devices along the ETICS façade shows a roughly consistent increase. The difference in temperature recorded with time for the respective devices does not show a drastic difference across scenarios. However, based on the gradient of the temperature–time curves of the devices, a slight increase in UFS rate can be detected when the EPS thickness is reduced. This is consistent with the previous UFS studies conducted to evaluate the impact of fuel thickness on UFS [42,43]. The highest temperatures were reached in scenario ETICS1 with an EPS thickness of 5 cm, with the maximum temperatures recorded at T1, T2, T3 and T4 being 529 °C, 160 °C, 77 °C and 63 °C, respectively. The corresponding maximum temperature values for the scenarios ETICS2 and ETICS3 were 513 °C, 156 °C, 73 °C and 61 °C, and 506 °C, 156 °C, 68 °C and 56 °C, respectively. These temperature values will increase over longer durations as the UFS was still incomplete in all three scenarios.
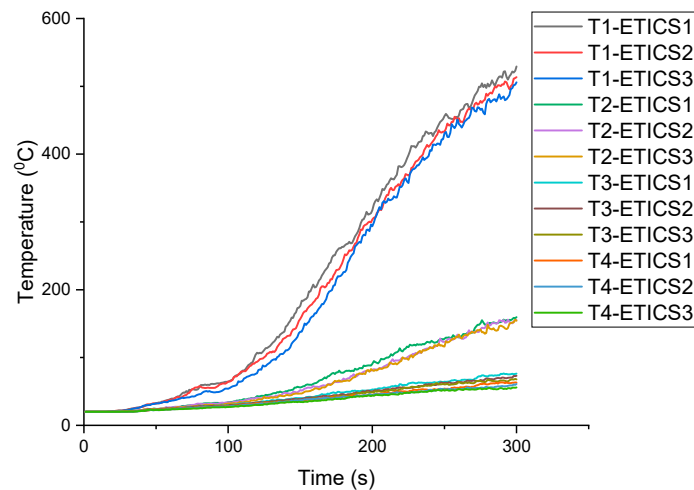
Figure 5. Variation in recorded temperature with time for the 3 scenarios of ETICS façade at Device T1, Device T2, Device T3 and Device T4.

The variation in temperature recorded with time in the 4 temperature devices for the 3 scenarios, DSF1, DSF2 and DSF3, is shown in Figure 6. The cavity widths in the 3 scenarios were 0.5 m, 1 m and 1.5 m, respectively.
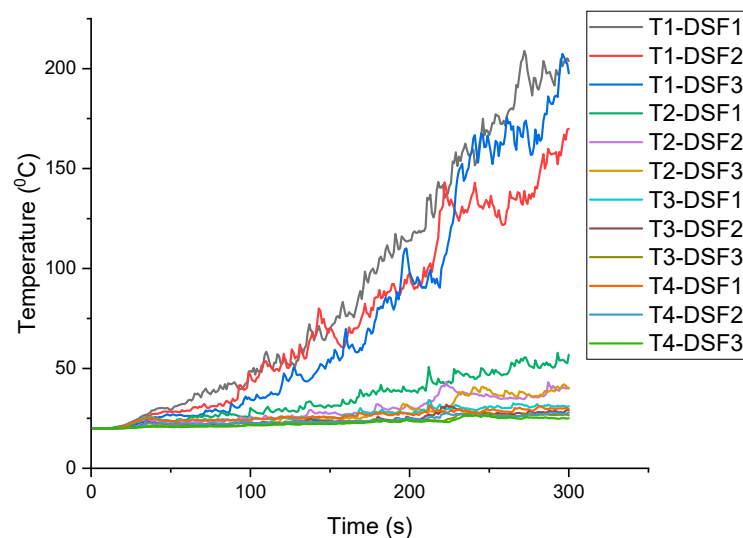

Figure 6. Variation in recorded temperature with time for the 3 scenarios of DSF at Device T1, Device T2, Device T3 and Device T4.

Within the simulation time of 300 s, the highest temperatures among all the devices were recorded for scenarios with a cavity width of 0.5 m. This result is consistent with the experimental results of Chow et al. [14]. Moreover, the gradient of the temperature–time curves recorded in all 4 devices suggests that the hot gases rise upwards fastest in scenario DSF1 with a cavity width of 0.5 m. The maximum temperatures recorded in scenarios DSF1 at T1, T2, T3 and T4 were 209 °C, 58 °C, 34 °C and 32 °C, respectively. The corresponding maximum temperature values in the scenarios DSF2 and DSF3 were 170 °C, 43 °C, 32 °C and 28 °C, and 207 °C, 42 °C, 28 °C and 27 °C, respectively.

The results from Figures 5 and 6 suggest that the UFS hazard is greatest in ETICS1 and DSF1 of the 6 scenarios simulated for the ETICS façade and DSF. The temperature recordings of ETICS1 and DSF1 were plotted along with the temperature recordings from the 3 VGS simulation scenarios in the same graph, as shown in Figure 7.
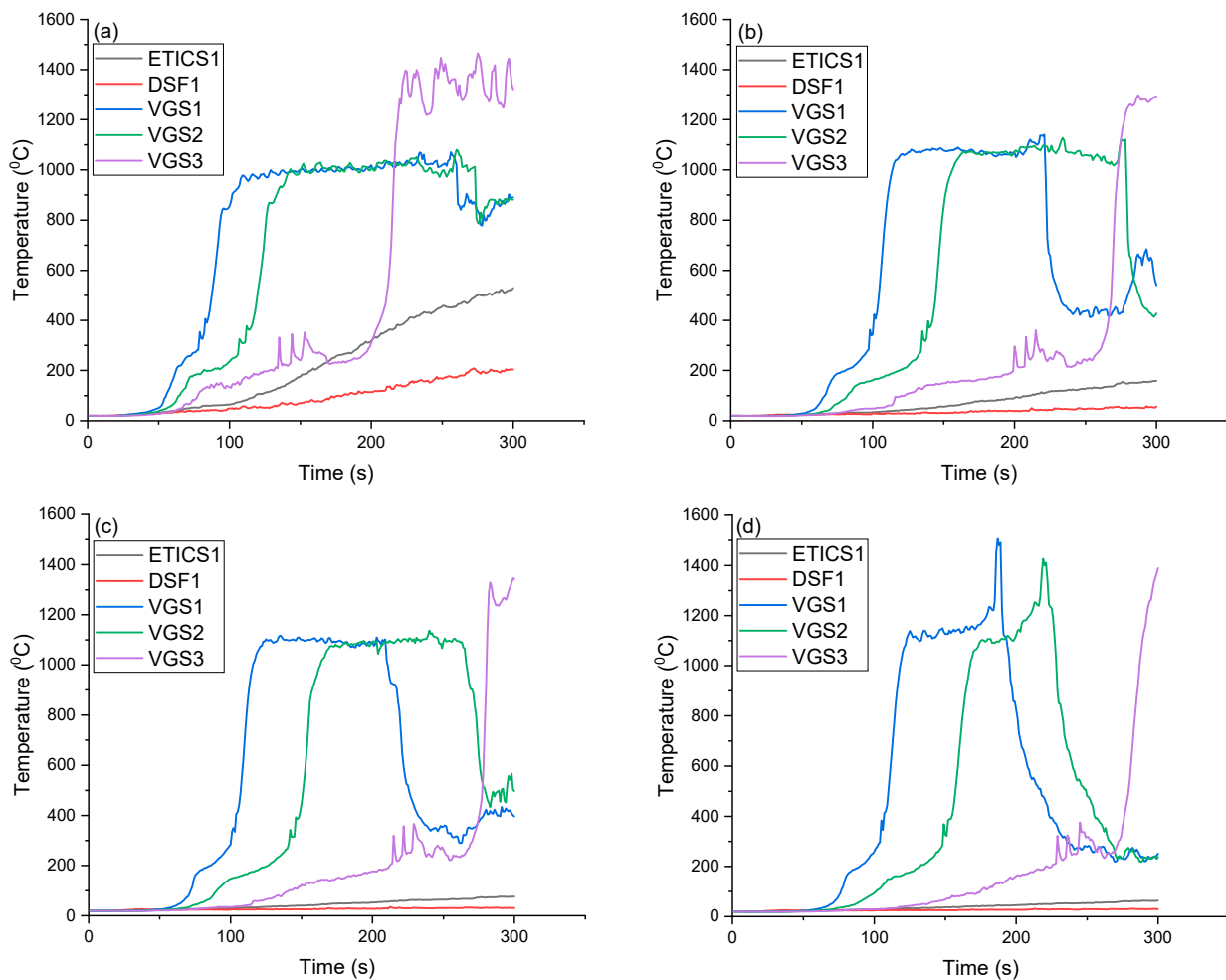
Figure 7. Variation in recorded temperature with time for the 3 scenarios of VGS along with ETICS1 and DSF1 at (**a**) Device T1, (**b**) Device T2, (**c**) Device T3 and (**d**) Device T4.

The temperature increase was rapid in all the devices along the VGS of all the 3 scenarios where MCs were 30%, 50% and 80%. The temperature recorded increased until it reached a roughly steady value and decreased sharply after remaining at the steady value for some time. By observing the gradient of the temperature–time curve, it can be concluded that the UFS is faster when the MC of vegetation is lower. The MC in vegetation acts as a heat sink to absorb heat via evaporation, which dilutes the flammable volatile pyrolyzates in the gas phase, and hinders the generation of a flammable mixture while partially blocking the air supply that is required for combustion [41]. Hence, the higher the MC, the lower the flammability and fire spread rate. The average UFS rates of the 3 scenarios, VGS1, VGS2 and VGS3, were 8.97 cms^{-1}, 5.51 cms^{-1} and 2.86 cms^{-1}, respectively.

Considering the scenarios simulated in this study, the UFS hazard of all three scenarios of VGS is higher than the scenarios with the highest UFS hazard from the ETICS and DSF. Fire spreads faster along the VGS wall and reaches higher temperature levels. The maximum temperature reached by all 4 devices (T1–T4) in all 3 VGS fire scenarios was more than 1000 °C, which was far more hazardous compared to the maximum temperatures of 529 °C and 209 °C reached by device T1 in ETICS1 and DSF1, respectively. The temperatures predicted in the FDS model used in this study were comparable to those found in previous studies for the same TEBFS [14,29,36]. The flame reached the device T4 which is 7 m above the broken window in 78 s, 127 s and 245 s at an average UFS rate of 8.97 cm/s, 5.51 cm/s and 2.86 cm/s, respectively, in the 3 scenarios VGS1, VGS2 and VGS3. However, within the simulation time of 300 s, the flame reached only close to 4 m and 1 m above the broken window in the scenarios ETICS1 and DSF1, respectively.

3.2. Temperature Distribution along the TEBFS

The temperature readings from the devices in each simulation scenario were analysed to evaluate their UFS hazard. These readings provide an understanding of how quickly the fire spreads along the TEBFS and the temperature reached at different heights of the façade. Moreover, the temperature SLICE animations generated in the Smokeview (SMV) visualisation tool help us to understand the nature of the temperature distribution along the TEBFS during the fire spread. SMV uses FDS output smoke and fire propagation data to produce animatic and graphical visualisations [44].

Flames and the hot gases from the room fire were observed to be moving upwards soon after ejecting from the window opening. A snapshot from the temperature distribution slice along the vertical plane in line with the façade in the 3 scenarios (ETICS1, DSF1 and VGS1) at the simulation time of 200 s is shown in Figure 8.
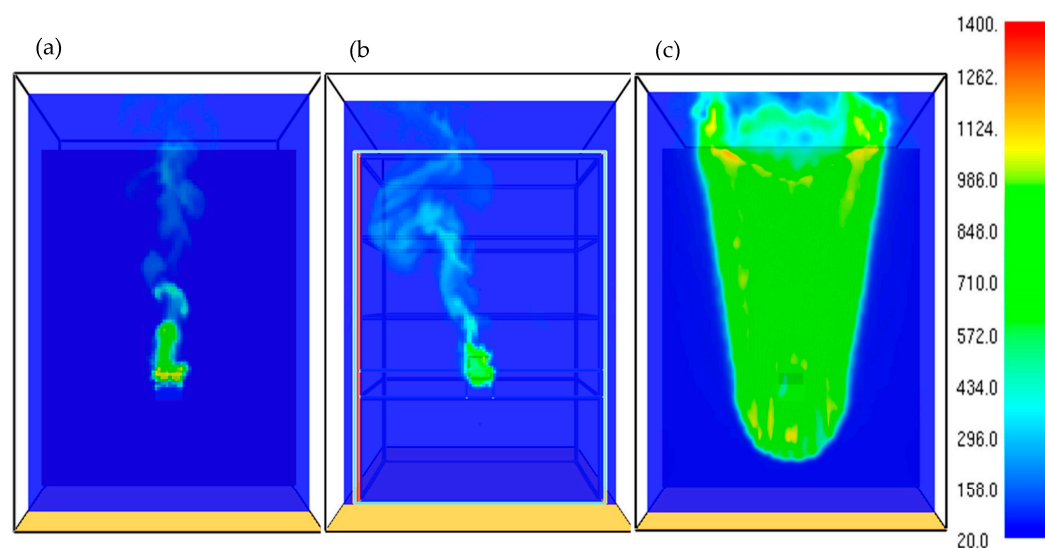

Figure 8. Vertical temperature distribution slice at simulation time 200 s of the scenarios (**a**) ETICS1, (**b**) DSF1, (**c**) VGS1.

In the 2 scenarios where combustion of façade material is taking place (ETICS1 and VGS1), the fire spreads upwards initially within the widths of the window opening. Thereafter, the fire spreads laterally towards the side edges of the façade, which has already begun in the VGS façade at 200 s. However, the UFS was not completed at 200 s in the ETICS façade, hence lateral fire spread is yet to be seen. Similarly, the flow of hot gases also took place predominantly in the upward direction in the DSF. Therefore, Figure 8 further highlights the faster UFS rate in VGS1 compared to ETICS1 and DSF1.

4. Conclusions

The UFS hazard of three TEBFS was evaluated using FDS models. Three scenarios were considered each for three TEBFS, namely, ETICS façade, DSF and VGS. EPS layer thickness, cavity width and vegetation MC were varied in the ETICS façade, DSF and VGS, respectively, to obtain different simulation scenarios. Numerical simulations were conducted using a 12 m tall building model in FDS, assuming a room fire of 1 MW followed by a window-ejected flame. The temperature along the vertical centreline of the TEBFS was recorded by placing temperature devices above the window at 4 heights: 5 m (T1), 7 m (T2), 9 m (T3) and 11 m (T4) from the base of the building. The UFS hazard of VGS fire scenarios was the greatest, which showed much faster UFS while recording higher temperatures along the wall. The times taken for the flame to reach T4 were 78 s, 127 s and 245 s, which are equivalent to average UFS rates of 8.97, 5.51 and 2.86 cms^{-1} in the 3 VGS scenarios. In contrast, the flame did not spread upwards beyond 4 m and 1 m above the broken window, within the simulation time of 300 s, in any of the scenarios of ETICS and

DSF, respectively. The maximum temperature recorded along all the temperature devices in all 3 VGS fire scenarios exceeded 1000 °C. The UFS hazards of the ETICS façade and DSF were comparatively lower. The maximum temperatures reached in the ETICS and DSF scenarios within the simulation time of 300 s were 529 °C and 209 °C, respectively. Even though these temperatures were comparable to past studies, it should be noted that their accuracy should be determined from real-scale experiments. Within the scope of this study, it is not a limitation as it intends only to determine the fire hazard of VGS in comparison to the ETICS façade and the DSF. Although not as hazardous as the UFS in the scenarios of VGS, the ETICS façade and DSF are scrutinised for their fire performance in building codes in many countries over the years due to the involved fire hazard. This study highlights the seriousness of the fire hazard involved with VGS with dried-out vegetation. The results of this study should not be used as a generalisation for the comparison of the UFS hazard of the three TEBFS considered in this study. Nevertheless, this study provides an important insight into how much of a fire hazard VGS can cause when dried to the MCs considered in this study, compared to the more established fire hazard scenarios of ETICS and DSF.

5. Limitations and Future Work

The selection of scenarios under each of the three TEFBSs is important when analysing the fire hazards among them. The differentiating factors in ETICS and DSF, which are EPS layer thickness and cavity width, are decided at the construction stage; whereas the differentiating factor in VGS scenarios, which is moisture content; depends on how the vegetation fuel bed is watered and maintained. The MC for the three scenarios simulated in this study was selected based on a study by Dahanayake and Chow [27]. In their study, three plant species commonly used in VGS; Hedera helix (HH), Peperomia obtusifolia (PO) and Aglaonema commutatum (AO); were subjected to natural drying. When watering was no longer carried out, the time taken by these 3 plant species to reach the MC levels used in the 3 simulation scenarios of this study is given in Table 5. It is assumed that the growing medium of the VGS is completely dry.

Table 5. Time taken by different vegetation species used in VGS to the MC levels considered in this study.

MC (%)	Time Taken to Reach the MC Level		
	HH	**PO**	**AO**
30%	15 days	62 days	More than 74 days
50%	13 days	58 days	More than 74 days
80%	11 days	55 days	More than 74 days

Table 5 shows that different vegetation species have different drying rates. Moreover, the thermal and physical properties of these vegetation species are also different, which affects their flammability and UFS hazard. Hence, the generalisation of the comparison of the UFS hazards of all VGS containing different vegetation species with other TEBFS like ETICS or DSF, is not very straightforward. The UFS hazard of VGS depends on many factors, such as the vegetation species used, the PR of the vegetation bed, the duration for which the vegetation is allowed to dry (which decides the MC of vegetation) and the ambient temperature and humidity during the period of drying. More studies based on experimental data and simulation results are necessary to generalise the comparison of the UFS hazard of different TEBFS.

Due to the high cost involved with conducting full-scale repetitive fire tests on three different façade systems, experimental data are not reported in this study. Nevertheless, the temperatures recorded in the FDS simulations in this study are comparable to the experimental results from previous studies conducted on ETICS [45], DSF [14] and VGS [29]. Even though the experimental setups reported in these studies are not an exact match to the FDS model used in the present study, the ranges of temperature recordings are

vastly comparable. While full-scale VGS fire experiments would be needed to validate the temperature values reported in this study, the values should be considered as estimates for evaluating the fire hazard of VGS compared to ETICS and DSF.

Author Contributions: Conceptualisation, T.L.W.K. and C.L.C.; methodology, T.L.W.K.; software, T.L.W.K.; validation, C.L.C.; formal analysis, T.L.W.K.; investigation, C.L.C.; resources, C.L.C.; data curation, T.L.W.K.; writing—original draft preparation, T.L.W.K.; writing—review and editing, C.L.C.; visualisation, T.L.W.K.; supervision, C.L.C.; project administration, C.L.C.; funding acquisition, C.L.C. All authors have read and agreed to the published version of the manuscript.

Institutional Review Board Statement: Not applicable.

Informed Consent Statement: Not applicable.

Data Availability Statement: No new data were created or analysed in this study. Data sharing is not applicable to this article.

Conflicts of Interest: The authors declare no conflict of interest. The funder had no role in the design of the study; in the collection, analysis or interpretation of data, in the writing of the manuscript or in the decision to publish the results.

References

1. Yildiz, Y.; Arsan, Z.D. Identification of the building parameters that influence heating and cooling energy loads for apartment buildings in hot-humid climates. *Energy* **2011**, *36*, 4287–4296. [CrossRef]
2. Kwok, Y.T.; Lau, K.; Ng, E. The Influence of Building Envelope Design on the Thermal Comfort of High-Rise Residential Buildings in Hong Kong. In Proceedings of the 10th Windsor Conference, Windsor Great Park, UK, 12–15 April 2018; pp. 1062–1075.
3. Rathnayake, U.; Lau, D.; Chow, C.L. Review on energy and fire performance of water wall systems as a green building façade. *Sustainability* **2020**, *12*, 8713. [CrossRef]
4. Hu, L.; Yang, T. Studies of fire prevention issues in exterior wall thermal insulation system. In Proceedings of the 2011 Second International Conference on Mechanic Automation and Control Engineering, Inner Mongolia, China, 15–17 July 2011; pp. 6104–6106.
5. Niziurska, M.; Wieczorek, M.; Borkowicz, K. Fire Safety of External Thermal Insulation Systems (ETICS) in the Aspect of Sustainable Use of Natural Resources. *Sustainability* **2022**, *14*, 1224. [CrossRef]
6. Chow, W.K.; Hung, W.Y. Effect of cavity depth on smoke spreading of double-skin façade. *Build. Environ.* **2006**, *41*, 970–979. [CrossRef]
7. Rathnayake, U.; Karunaratne, T.L.W.; Han, S.; Lau, D.; Chow, C.L. Experimental investigation on thermal performance of water wall systems exposed to fire. *Indoor Built Environ.* **2022**, *32*, 170–182. [CrossRef]
8. Lee, Y.-P.; Delichatsios, M.A.; Silcock, G.W.H. Heat fluxes and flame heights in façades from fires in enclosures of varying geometry. *Proc. Combust. Inst.* **2007**, *31*, 2521–2528. [CrossRef]
9. Chow, N.C.L.; Li, S.S.; Huang, D.X. Apron design for protecting double-skin façade fires. *Fire Mater.* **2015**, *39*, 189–206. [CrossRef]
10. Huang, Y.; Yeboah, S.; Shao, J. Numerical investigation of fire in the cavity of naturally ventilated double skin façade with venetian blinds. *Build. Serv. Eng. Res. Technol.* **2022**, *44*, 45–61. [CrossRef]
11. Yanagisawa, A.; Goto, D.; Ohmiya, Y.; Delichatsios, M.A.; Lee, Y.-P.; Wakatsuki, K. Effect of a facing wall on façade flames. In Proceedings of the Fire Safety Science—9th International Symposium, Karlsruhe, Germany, 21–26 September 2008; pp. 801–811.
12. Miao, L.; Chow, C.L. A study on window plume from a room fire to the cavity of a double-skin façade. *Appl. Therm. Eng.* **2018**, *129*, 230–241. [CrossRef]
13. Chow, C.L. Numerical studies on smoke spread in the cavity of a double-skin façade. *J. Civ. Eng. Manag.* **2011**, *17*, 371–392. [CrossRef]
14. Chow, W.K.; Hung, W.Y.; Gao, Y.; Zou, G.; Dong, H. Experimental study on smoke movement leading to glass damages in double-skinned façade. *Constr. Build. Mater.* **2007**, *21*, 556–566. [CrossRef]
15. An, W.; Wang, Z.; Xiao, H.; Sun, J.; Liew, K.M. Thermal and fire risk analysis of typical insulation material in a high elevation area: Influence of sidewalls, dimension and pressure. *Energy Convers. Manag.* **2014**, *88*, 516–524. [CrossRef]
16. Zhang, Y.; Sun, J.H.; Huang, X.J.; Chen, X.F. International Journal of Heat and Mass Transfer Heat transfer mechanisms in horizontal flame spread over wood and extruded polystyrene surfaces. *Int. J. Heat Mass Transf.* **2013**, *61*, 28–34. [CrossRef]
17. Peng, L.; Ni, Z.; Huang, X. Review on the Fire Safety of Exterior Wall Claddings in High-rise Buildings in China. *Procedia Eng.* **2013**, *62*, 663–670. [CrossRef]
18. McKenna, S.T.; Jones, N.; Peck, G.; Dickens, K.; Pawelec, W.; Oradei, S.; Harris, S.; Stec, A.A.; Hull, T.R. Fire behaviour of modern façade materials—Understanding the Grenfell Tower fire. *J. Hazard. Mater.* **2019**, *368*, 115–123. [CrossRef] [PubMed]

19. Zhou, B.; Yoshioka, H.; Noguchi, T.; Wang, K.; Huang, X. Upward Fire Spread Rate Over Real-Scale EPS ETICS Façades. *Fire Technol.* **2021**, *57*, 2007–2024. [CrossRef]

20. Ezinwa, J.U.; Robson, L.D.; Obach, M.R.; Torvi, D.A.; Weckman, E.J. Evaluating Models for Predicting Full-Scale Fire Behaviour of Polyurethane Foam Using Cone Calorimeter Data. *Fire Technol.* **2014**, *50*, 693–719. [CrossRef]

21. Pitts, W.M. Role of two stage pyrolysis in fire growth on flexible polyurethane foam slabs. *Fire Mater.* **2014**, *38*, 323–338. [CrossRef]

22. D'Souza, M.V.; McGuire, J.H. ASTM E-84 and the flammability of foamed thermosetting plastics. *Fire Technol.* **1977**, *13*, 85–94. [CrossRef]

23. Hadden, R.; Alkatib, A.; Rein, G.; Torero, J.L. Radiant Ignition of Polyurethane Foam: The Effect of Sample Size. *Fire Technol.* **2014**, *50*, 673–691. [CrossRef]

24. Wong, N.H.; Tan, A.Y.K.; Tan, P.Y.; Sia, A.; Wong, N.C. Perception studies of vertical greenery systems in Singapore. *J. Urban Plan. Dev.* **2010**, *136*, 330–338. [CrossRef]

25. Pérez, G.; Rincón, L.; Vila, A.; González, J.M.; Cabeza, L.F. Green vertical systems for buildings as passive systems for energy savings. *Appl. Energy* **2011**, *88*, 4854–4859. [CrossRef]

26. Chew, M.Y.L.; Conejos, S.; Azril, F.H. Bin Design for maintainability of high-rise vertical green facades. *Build. Res. Inf.* **2019**, *47*, 453–467. [CrossRef]

27. Dahanayake, K.C.; Chow, C.L. Moisture Content, Ignitability, and Fire Risk of Vegetation in Vertical Greenery Systems. *Fire Ecol.* **2018**, *14*, 125–142. [CrossRef]

28. Dahanayake, K.C.; Yang, Y.; Wan, Y.; Han, S.; Chow, C.L. Study on the fire growth in underground green corridors. *Build. Simul.* **2020**, *13*, 627–635. [CrossRef]

29. Karunaratne, T.L.W.; Chow, C.L. Fire spread along vertical greenery systems from window ejected flame: A study based on a fire dynamic simulator model. *J. Build. Eng.* **2022**, *62*, 105359. [CrossRef]

30. Anderson, W.R.; Catchpole, E.A.; Butler, B.W. Convective heat transfer in fire spread through fine fuel beds. *Int. J. Wildl. Fire* **2010**, *19*, 284–298. [CrossRef]

31. McGrattan, K.; Hostikka, S.; McDermott, R.; Floyd, J.; Weinschenk, C.; Overhold, K. *Fire Dynamics Simulator User 's Guide (FDS)*, 6th ed.; NIST Spec. Publ. 1019; National Institute of Standards and Techology: Gaithersburg, MD, USA, 2020.

32. Cicione, A.; Walls, R.S. Towards a simplified fire dynamic simulator model to analyse fire spread between multiple informal settlement dwellings based on full-scale experiments. *Fire Mater.* **2021**, *45*, 720–736. [CrossRef]

33. Karlsson, B.; Quintiere, J.G. *Enclosure Fire Dynamics*; CRC Press: New York, NY, USA, 1999.

34. Ahmadi, O.; Mortazavi, S.B.; Pasdarshahri, H.; Mohabadi, H.A. Consequence analysis of large-scale pool fire in oil storage terminal based on computational fluid dynamic (CFD). *Process Saf. Environ. Prot.* **2019**, *123*, 379–389. [CrossRef]

35. Zhou, B.; Yoshioka, H.; Noguchi, T.; Ando, T. Numerical prediction of mass loss rate of expanded polystyrene (EPS) used for external thermal insulation composite systems (ETICS) in cone calorimeter. *Fire Mater.* **2018**, *42*, 517–526. [CrossRef]

36. Chow, C.L. Full-scale burning tests on double-skin façade fires. *Fire Mater.* **2013**, *37*, 17–34. [CrossRef]

37. Nilica, R.; Harmuth, H. Mechanical and fracture mechanical characterization of building materials used for external thermal insulation composite systems. *Cem. Concr. Res.* **2005**, *35*, 1641–1645. [CrossRef]

38. Stoliarov, S.I.; Crowley, S.; Lyon, R.E.; Linteris, G.T. Prediction of the burning rates of non-charring polymers. *Combust. Flame* **2009**, *156*, 1068–1083. [CrossRef]

39. Jayalakshmy, M.S.; Philip, J. Thermophysical properties of plant leaves and their influence on the environment temperature. *Int. J. Thermophys.* **2010**, *31*, 2295–2304. [CrossRef]

40. Simpson, W.; TenWolde, A. Physical properties and moisture relations of wood. In *Wood Handbook: Wood as An Engineering Material*; General Technical Report FPL; GTR-113; USDA Forest Service, Forest Products Laboratory: Madison, WI, USA, 1999; pp. 3.1–3.24.

41. Park, W.C.; Atreya, A.; Baum, H.R. Determination of pyrolysis temperature for charring materials. *Proc. Combust. Inst.* **2009**, *32*, 2471–2479. [CrossRef]

42. Jiang, L.; He, J.J.; Sun, J.H. Sample width and thickness effects on upward flame spread over PMMA surface. *J. Hazard. Mater.* **2018**, *342*, 114–120. [CrossRef]

43. McAllister, S.; Grenfell, I.; Hadlow, A.; Jolly, W.M.; Finney, M.; Cohen, J. Piloted ignition of live forest fuels. *Fire Saf. J.* **2012**, *51*, 133–142. [CrossRef]

44. Chow, W.K.; Chow, C.L.; Li, S.S. Simulating smoke filling in big halls by computational fluid dynamics. *Model. Simul. Eng.* **2011**, *2011*, 781252. [CrossRef]

45. Yakovchuk, R.; Kuzyk, A.; Skorobagatko, T.; Yemelyanenko, S.; Borys, O.; Dobrostan, O. Computer simulation of fire test parameters façade heat insulating system for fire spread in fire dynamics simulator (FDS). *Ser. Geol. Technol. Sci.* **2020**, *4*, 35–44. [CrossRef]